Extreme violation of the Leggett-Garg inequality in nonunitary dynamics with complex energies

Anant V. Varma,[1,*] Jacob E. Muldoon,[2,†] Sourav Paul,[1,‡] Yogesh N. Joglekar,[2,§] and Sourin Das[1,∥]

[1]*Indian Institute of Science Education and Research Kolkata, Mohanpur, Nadia 741246, West Bengal, India*
[2]*Department of Physics, Indiana University Purdue University Indianapolis (IUPUI), Indianapolis, Indiana 46202, USA*

We study the Leggett-Garg inequality (LGI) of a two-level system (TLS) undergoing coherent dynamics described by a non-Hermitian Hamiltonian and Lindblad equation with no quantum jumps. The nonlinear Bloch equation for the TLS density matrix predicts violations of LGI above the TLS Lüders bound of 3/2, approaching the extremal case of LGI parameter $K_3 = 3$ in the $\mathcal{PT}$-symmetric region and the $\mathcal{PT}$-broken region. We show that these findings are reproduced by using postselection to remove instantaneous quantum jumps from a three-level system described by the Lindblad equation with a single spontaneous emission dissipator. We trace the K_3 excesses beyond the standard quantum limit of 3/2 to a nonuniform speed of evolution on the Bloch sphere. Finally, we consider the effects of competing Lindblad dissipators on the postselected non-Hermitian dynamics and the viability of observing K_3 exceeding the Lüder bound and approaching its algebraic maximum of three in current experimental setups.

I. INTRODUCTION

Our intuition of the classical world is embodied by twin postulates of macroscopic realism and noninvasive measurability [1]. The first relates to the assumption that for macroscopic systems, observables—position, momentum, energy—have pre-existing values. The second encodes the assumption that these observables can be measured to an arbitrary accuracy without affecting their values. The inapplicability of these two postulates signals the transition from a classical system to the quantum domain, and it can be identified through spatiotemporal correlation functions of different observables for the system in question. Traditional Bell inequalities reference correlations between spatially separated, equal-time measurements of a multipartite quantum system with at least two qubits [2,3]. On the other hand, the "quantumness" or quantum-to-classical transition of a minimal quantum system (a single qubit) is characterized by Leggett-Garg inequalities (LGIs) which utilize temporal correlations [4–6]. Violation of a suitable set of Leggett-Garg inequalities is one of the well-established markers of quantum dynamics [2,3,7–9], when supplemented with no signaling in time and arrow of time conditions [10,11]. These inequalities have been exploited to test quantum mechanics at macroscopic scales in experimental platforms such as a superconducting circuit [12,13], light-matter interface [14], and heralded single photons [15].

The simplest LGI describes a three-time protocol where a dichotomic observable Q with outcomes $a = \{+1, -1\}$ is measured at times $t_0 \leqslant t_1 \leqslant t_2$ in a pairwise fashion. The LGI then provides a bound on the parameter $K_3 \equiv C_{01} + C_{12} - C_{02}$, where $C_{ij} = \sum_{ab} ab P_{ij}(a, b)$ is the correlation function and $P_{ij}(a, b)$ is the joint probability of obtaining the result a at time t_i and result b at a later time t_j. For a quantum system with Hermitian Hamiltonian $H_0 = H_0^\dagger$ initialized in the state $|\psi(0)\rangle$, the two-time correlation function is related to the anticommutator of the Heisenberg-picture observable $Q(t) = e^{iH_0 t} Q e^{-iH_0 t}$ ($\hbar = 1$) by $C_{ij} = \langle\psi(0)|\{Q(t_i), Q(t_j)\}|\psi(0)\rangle/2$ [16]. Since each $|C_{ij}| \leqslant 1$, the LGI metric K_3 is algebraically bounded by ± 3. The postulates of macroscopic realism and noninvasive measurability imply that $K_3 \leqslant 1$ for a classical system. This classical bound is violated when operators $Q(t_i)$ and $Q(t_j)$ do not commute, leading to a maximum value $K_3 = 3/2$ for the three-time protocol and $K_N = N \cos(\pi/N)$ for its N-time generalization [9,16]. For a two-level system (TLS) undergoing unitary dynamics, the Lüders bound $K_3^L = 3/2$ saturates the K_3 value; the corresponding bound is higher in an $M > 2$-level system, with the algebraic limit $K_3 \to 3$ achieved in the $M \to \infty$ limit [17].

When a small (M-dimensional) quantum system is coupled to an environment, the dynamics for the reduced density matrix of the system (not the environment) is given by a completely positive trace preserving (CPTP) map [18–24]. This map is characterized by M^2 Kraus operators and, in the most common case of an environment with no memory, is equivalent to the time evolution generated by the Gorini-Kossakowski-Sudarshan Lindblad equation (henceforth the Lindblad equation) for the reduced density matrix [25]. The CPTP maps can be divided into unital (which leaves a maximally mixed state unchanged) and nonunital ones. For two-level systems, $M = 2$, the maximal violation of the LGI is constrained to the Lüders bound ($K_3^L = 3/2$) for unitary dynamics [4,9,16] and decoherence-inducing unital maps [26].

In this article, we show that for a two-level system governed by a non-Hermitian Hamiltonian, the LGI

*anantvijay.cct@gmail.com
†jemuldoo@iupui.edu
‡sp20rs034@iiserkol.ac.in
§yojoglek@iupui.edu
∥sourin@iiserkol.ac.in; sdas.du@gmail.com

parameter $K_3(t_0, t_1, t_2; Q, H, |\psi(0)\rangle)$, optimized over the parameter space, exceeds the Lüder bound and reaches its algebraic maximum of three over a wide parameter range. Such a Hamiltonian is experimentally realized in minimal quantum systems undergoing *nonunital* CPTP evolution by postselecting to no-quantum-jump trajectories [27]. With a three-level superconducting circuit in mind, we obtain the analytical expressions for the dynamics of the postselected two-level system that evolves with a non-Hermitian Hamiltonian. In the special case when the resultant non-Hermitian Hamiltonian has an antilinear symmetry, traditionally called the parity-time ($\mathcal{PT}$) symmetry, the energy spectrum of H is either real or complex-conjugate pairs. The transition from a $\mathcal{PT}$-symmetric phase (real energies) into $\mathcal{PT}$-broken phase (complex conjugate energies) occurs across an exceptional point (EP) degeneracy where the corresponding eigenvectors also coalesce. When the spectrum of H is real, max $K_3 \to 3$ in the vicinity of the EP, but only at divergent times, $\Delta t_{01} \equiv t_1 - t_0 \to \infty$ [28–30]. Here we show that K_3 exceeds the Lüder bound and approaches three at moderate times Δt over a broad range of parameters in the $\mathcal{PT}$-broken region. These extreme correlations are understood by calculating the maximum and minimum speed of state evolution under trace-preserving, nonlinear, non-Hermitian dynamics that occur in the postselected manifold in the absence of quantum jumps. Lastly, by comparing the results of coherent, non-Hermitian dynamics with those from the three-level system Lindblad analysis, we show that the extremal correlations are only weakly affected by additional dissipation channels or coherent drives.

The article is organized as follows. In Sec. II, we present the model and obtain two-time joint probabilities $P_{ij}(a, b)$ for a two-level, non-Hermitian system, as well as the underlying three-level, open dissipative quantum system that undergoes Lindblad evolution. This is followed by numerical results for the optimized K_3 values across the parameter space. The dynamics of the non-Hermitian TLS is discussed in Sec. III, along with the role of the nonlinear Bloch equation of motion in generating nonuniform speed of evolution (SOE). We present the effects of hitherto ignored, experimentally relevant dissipators on the Leggett-Garg (LG) parameter K_3 in Sec. IV, and present conclusions in Sec. V.

II. NON-HERMITIAN AND LINDBLAD MODELS

Consider a two-level system (a qubit) governed by a non-Hermitian Hamiltonian $H = H_0 - i\Gamma$ where $H_0 = H_0^\dagger$ denotes its Hermitian part and $i\Gamma = -(i\Gamma)^\dagger$ denotes its anti-Hermitian part. When Γ is positive definite, such a Hamiltonian arises naturally from a larger, open quantum system and represents lossy dynamics. On the other hand, when Γ has zero trace, it represents a balanced gain and loss system whose dynamics can be mapped onto the lossy-dynamics systems by a time-dependent rescaling of the density matrix. As an explicit example, we will use the classic, balanced gain-loss Hamiltonian

$$H(\gamma) = -\frac{J}{2}\sigma_x + i\frac{\gamma}{2}\sigma_z \equiv \vec{A} \cdot \sigma + i\vec{B} \cdot \sigma. \quad (1)$$

It is straightforward to check that $H(\gamma)$ is $\mathcal{PT}$ symmetric with parity operator $\mathcal{P} = \sigma_x$ and canonical complex

conjugation, i.e., $\mathcal{T} = *$. The eigenvalues of $H(\gamma)$ are given by $\epsilon_\pm = \pm\sqrt{J^2 - \gamma^2}/2$ and therefore change from purely real for $J \geqslant \gamma$ to complex-conjugate pair for $J < \gamma$. The corresponding Dirac-normalized right eigenvectors $|\epsilon_\pm\rangle$ have equal weight in both levels when $J > \gamma$, indicating a $\mathcal{PT}$-symmetric phase. For $J < \gamma$, the ratio of weights in the two levels is exponentially amplified or suppressed for the two eigenvectors. Therefore, in the $\mathcal{PT}$-symmetry broken region, the action of the $\mathcal{PT}$ operation maps one eigenvector into another. The Dirac inner product of the two linearly independent eigenvectors is given by $|\langle\epsilon_+|\epsilon_-\rangle| = \min(\gamma/J, J/\gamma)$. It reaches unity at the EP $\gamma = J$.

In order to calculate the LGI parameter $K_3(t_0, t_1, t_2)$, we use a measurement operator $Q = \sigma_y$ that is orthogonal to the Hermitian and the anti-Hermitian parts of the Hamiltonian. Incidentally, we also note that the Hamiltonian $H = H_0 - i\Gamma$ is $\mathcal{PT}$ symmetric if and only if the operators H_0 and Γ are orthogonal to each other (under the Frobenius inner product), i.e., $\vec{A} \cdot \vec{B} = 0$. For a Hermitian system, the joint probabilities $P_{ij}(a, b)$ would ordinarily be constructed from the inner products between the time-evolved states $|\psi(t_i - t_0)\rangle$ or $|\psi(t_j - t_i)\rangle$ and the measurement states $|a\rangle$ and $|b\rangle$, respectively. However, when the time-evolution operator $G_{ij} \equiv \exp[-iH(\gamma)(t_j - t_i)]$ is not unitary, we must normalize each measurement accordingly. Doing so yields

$$P_{ij}(a, b) = \frac{|\langle b|G_{ij}|a\rangle|^2}{|\langle a|G_{ij}^\dagger G_{ij}|a\rangle|} \frac{|\langle a|G_{0i}|\psi_0\rangle|^2}{|\langle\psi_0|G_{0i}^\dagger G_{0i}|\psi_0\rangle|}. \quad (2)$$

The two-point correlations $C_{ij} = \sum_{ab} ab P_{ij}(a, b)$ and the LGI parameter $K_3 = C_{01} + C_{12} - C_{02}$ are then calculated from the joint probabilities, Eq. (2). Equivalently, we seek a trace-preserving dynamical equation for the Dirac-Hermitian density matrix $\rho(t) = \rho(t)^\dagger$ of the system that is undergoing a coherent but nonunitary evolution generated by $H_0 - i\Gamma$. It is given by [31]

$$\partial_t \rho(t) = -i[H_0, \rho(t)] - \{\Gamma, \rho(t)\} + 2\mathrm{Tr}[\rho(t)\Gamma]\rho(t), \quad (3)$$

where $\{\cdot, \cdot\}$ denotes the anticommutator, and its solution is given by

$$\rho(t) = \frac{\mathbb{I} + \vec{S}(t) \cdot \vec{\sigma}}{2} = \frac{G(t)\rho_0 G^\dagger(t)}{\mathrm{Tr}[G(t)\rho_0 G^\dagger(t)]}, \quad (4)$$

where t represents the time interval $t_i - t_0$ or $t_j - t_i$.

Figure 1(a) shows the K_3 values for a system initialized in $|\psi(0)\rangle = (1, i)^T/\sqrt{2}$, i.e., an eigenstate $|+_y\rangle$ of the measurement operator $Q = \sigma_y$, obtained by choosing $t_0 = 0$, $t_j = 2t = 2t_i$ as a function of dimensionless time γt and inverse non-Hermiticity J/γ. We choose γ as the energy (frequency) scale because in experimentally accessible minimal quantum systems such as a superconducting circuit [27], it is determined by parameters that are not easily tunable, whereas the Hermitian Rabi drive strength J can be dynamically varied at will.

In the Hermitian limit ($J/\gamma \gg 1$), we observe the expected periodic behavior of the K_3 value, where the possible quantum mechanical behavior characterized by $1 \leqslant K_3 \leqslant 3/2$ is obtained in the first and last quarter of the period. As the drive strength is decreased, in the $\mathcal{PT}$-symmetric region ($J/\gamma > 1$), the system undergoes periodic behavior with
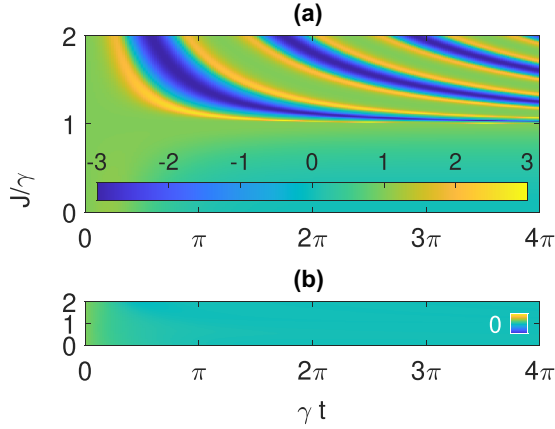
FIG. 1. LGI parameter $K_3(0, t, 2t)$ for a fixed observable $Q = \sigma_y$ and initial state $|\psi(0)\rangle = |+_y\rangle$ as a function of unit less time γt and inverse non-Hermiticity J/γ. (a) Equation of motion approach, Eq. (3), for a two-level system with Hamiltonian $H(\gamma)$ shows K_3 varying periodically in time with a period that diverges as the system approaches the EP at $J = \gamma$ from the Hermitian-limit side. Regions of K_3 that exceed the Lüder bound of $3/2$ are clearly seen with $K_3 \to 3$ at the transition point. In the $\mathcal{PT}$-symmetry broken region $J/\gamma < 1$, the *nonoptimized* LGI parameter K_3 reaches zero at long times $\gamma t \gg 1$. (b) The LGI parameter K_3 is calculated using Lindblad dynamics for a three-level system, Eq. (5), and shows a rapid decay to zero at times $\gamma t \sim 1$.

period $T(\gamma) = 2\pi/(\epsilon_+ - \epsilon_-) = 2\pi/\sqrt{J^2 - \gamma^2}$ and the resultant oscillations in K_3 also reach values that exceed the Lüders bound. It is important to note that the time at which such violation occurs increases monotonically as the system gap $\epsilon_+ - \epsilon_-$ is suppressed. As we approach the exceptional point $\gamma = J$, the LGI parameter K_3 reaches its algebraic maximum, $K_3 \to 3$, albeit at divergingly long times. In the $\mathcal{PT}$-broken region, on the other hand, for this choice of measurement operator $Q = \sigma_y$ and initial state $|\psi(0)\rangle = |+_y\rangle$, the K_3 rapidly decreases towards zero, indicating complete decoherence. The results in Fig. 1(a) show that a *non-Hermitian* two-level system violates the Lüders bound that has been well established for unitary dynamics (isolated quantum systems) as well as unital CPTP maps (open quantum systems with specific system-bath couplings or dissipators). However, this violation occurs at long times $\gamma t \gg 1$ where the validity of the non-Hermitian Hamiltonian description of the system becomes increasingly tenuous.

To understand the limits of non-Hermitian Hamiltonian description for a two-level system with no classical counterpart (not a two-mode system), we start with a three-level quantum system coupled to an environment. The three-dimensional density matrix $\rho_3(t)$ for this system is obtained by unitary evolution of the system plus environment density matrix, followed by tracing out the environment degrees of freedom [25]. In the presence of a memoryless environment, this generates decoherence for the (reduced) density matrix $\rho_3(t)$ whose dynamics are described by the Lindblad equation,

$$\partial_t \rho_3(t) = -i[H_3, \rho] - \frac{1}{2} \sum_{\alpha=1}^{3^2-1} \gamma_\alpha \mathcal{D}_\alpha(\rho_3) \equiv \mathcal{L}(\rho_3), \quad (5)$$

$$\mathcal{D}_\alpha(\rho_3) = \{L_\alpha^\dagger L_\alpha, \rho\} - 2L_\alpha \rho L_\alpha^\dagger. \quad (6)$$

Here, $H_3 = H_3^\dagger$ is the Hermitian Hamiltonian that acts only on the three-level system, and L_α are the Lindblad dissipators with strengths $\gamma_\alpha > 0$ that result from the partial-trace operation. $\mathcal{D}_\alpha$ are traceless, nonlinear operators, Eq. (6), that represent coherent, non-trace-preserving dynamics generated by the anticommutator term $\{\cdot, \cdot\}$ and trace-correcting quantum jump terms that generate decoherence.

Since Eq. (5) is linear in the density matrix, it is solved most easily by vectorizing the density matrix $\rho \to |\rho^v\rangle$. We convert the density matrix ρ_3 by stacking its columns into a 3^2-dimensional vector $|\rho^v\rangle$ [32]. As a result, the operator bilinears $A\rho_3 B$ are mapped to $B^T \otimes A|\rho^v\rangle$ and the Frobenius inner product on the matrix space devolves to a Dirac inner product for their vectorized counterpart, $\text{Tr}(\rho_1^\dagger \rho_2) = \langle \rho_1^v | \rho_2^v \rangle$ [32]. Thus, Eq. (5) becomes $\partial_t |\rho^v(t)\rangle = \mathcal{L}|\rho^v(t)\rangle$, where the matrix $\mathcal{L}$ is given by

$$\mathcal{L} = -i[\mathbf{1} \otimes H_3 - H_3^T \otimes \mathbf{1}]$$
$$- \sum_\alpha \frac{\gamma_\alpha}{2}[\mathbf{1} \otimes L_\alpha^\dagger L_\alpha + (L_\alpha^\dagger L_\alpha)^T \otimes \mathbf{1} - 2L_\alpha^* \otimes L_\alpha]. \quad (7)$$

Therefore, the time-dependent density matrix is obtained as $|\rho^v(t)\rangle = \exp(\mathcal{L}t)|\rho^v(0)\rangle \equiv \mathcal{G}(t)|\rho^v\rangle$. The relevant joint probabilities $P_{ij}(a, b)$ are obtained by projecting onto orthonormal density matrices $\rho_a \equiv |a\rangle\langle a|$ and $\rho_b = |b\rangle\langle b|$, respectively. To connect this general theory to a non-Hermitian two-level system, we consider a superconducting junction that is dispersively coupled to a cavity, with the three energy levels labeled as $|g\rangle$ (ground state), $|e\rangle$ (first excited state), and $|f\rangle$ (second excited state). When the levels $|e\rangle - |f\rangle$ are driven on resonance by a microwave drive with strength J, in the rotating wave approximation, the Hamiltonian H_3 is given by

$$H_3 = -\frac{J}{2}(|e\rangle\langle f| + |f\rangle\langle e|) + E_g|g\rangle\langle g|, \quad (8)$$

where the average of the two excited state energies is the zero of the energy, and $E_g < 0$ denotes the ground state energy. In principle, the Lindblad description of this system has $3^2 - 1 = 8$ possible dissipators L_α. We focus on the case where spontaneous emission (quantum jump) from the $|e\rangle$ to the $|g\rangle$ is the most dominant one. The dissipator corresponding to this process is given by $L_{ge} \equiv |g\rangle\langle e|$ and we will denote its strength as γ. We note that the CPTP map produced by this dissipator is *not unital* [26]. We use $Q = i(|e\rangle\langle f| - |f\rangle\langle e|)$ as the measurement operator and $|\psi(0)\rangle = (|e\rangle + i|f\rangle)/\sqrt{2}$ as the initial state, thereby mimicking a two-level system in the $|e\rangle - |f\rangle$ manifold.

Figure 1(b) shows the numerically calculated LGI parameter K_3 for this system as a function of inverse non-Hermiticity J/γ and a shorter range of dimensionless time γt. As is expected for an open system that will end up in the ground state due to spontaneous emission at times $\gamma t \sim 1$, the $K_3(t)$ rapidly approaches zero.

How does one then obtain coherent, non-Hermitian dynamics in such a qutrit undergoing Lindblad evolution? It is by ignoring the quantum jumps. In experiments, this means we only keep quantum trajectories where the single-shot measurement of the qutrit's energy registers it in the manifold of the two excited states [27,33]. Since the qutrit eventually decays to the ground state by spontaneous emission, the

fraction of eligible trajectories reduces exponentially with time [34]. Theoretically, the no-quantum-jump condition is given by $L_{ge}\rho_3(t)L_{ge}^\dagger = 0$. Under this constraint, the equation of motion for the density matrix becomes $\partial_t \rho_3 = -i(H_3'\rho_3 - \rho_3 H_3'^\dagger)$ with an effective, non-Hermitian Hamiltonian $H_3' = H_3 - i\gamma |e\rangle\langle e|$. When the density matrix ρ_3 and all relevant operators including H_{eff} are projected onto the subspace spanned by the $|f\rangle - |e\rangle$ manifold, the dynamics of the resultant 2×2 density matrix $\rho(t)$ are described by the lossy version of the $\mathcal{PT}$-symmetric Hamiltonian Eq. (1),

$$H_{\text{eff}} = H(\gamma) - i\frac{\gamma}{2}\mathbb{I}. \qquad (9)$$

The results for the LGI parameter K_3 are obtained by calculating $|\rho^v(t)\rangle$ and using it to obtain the joint probabilities as

$$P_{ij}(a, b) = \frac{\langle \rho_b^v | \mathcal{G}_{ij} | \rho_a^v \rangle}{1 - \langle \rho_g^v | \mathcal{G}_{ij} | \rho_a^v \rangle} \frac{\langle \rho_a^v | \mathcal{G}_{0i} | \rho^v(0) \rangle}{1 - \langle \rho_g^v | \mathcal{G}_{0i} | \rho^v(0) \rangle}. \qquad (10)$$

As expected, the results obtained are identical to those in Fig. 1(a). The contrast between the full-Lindblad results, Fig. 1(b), and those obtained from no-quantum-jump postselection shows that the coherent, nonunitary dynamics generated by a non-Hermitian Hamiltonian provides an alternate avenue to maximize temporal quantum correlations. We remind the reader that K_3 values in Fig. 1 are for a fixed measurement operator and initial state, and thus are not optimized.

To optimize the LG parameter K_3 across the exceptional point, we numerically obtain its dependence on an arbitrary initial state $|\psi(\theta, \phi)\rangle = (\cos\frac{\theta}{2}, e^{i\phi}\sin\frac{\theta}{2})^T$ and a dichotomous measurement operator $Q = \hat{m} \cdot \vec{\sigma}$ with $\hat{m} = (\sin\theta_m \cos\phi_m, \sin\theta_m \sin\phi_m, \cos\theta_m)$. We also assume that $t_0 = 0$ and $t_1 - t_0 = t_2 - t_1 = t$, where the measurements are made at three time instants $t_0 = 0, t_1 = t$, and $t_2 = 2t$. We then numerically optimize the expression of $K_3(t)$ over the complete parameter space comprised of four parameters $\{\theta, \phi, \theta_m, \phi_m\}$, for a fixed value of γ/J. Figure 2 shows the results of this calculation.

For $\gamma/J > 0$, we find that max K_3 is always greater than the Lüders bound of $3/2$ for a two-level system. Moreover, as we move across the exceptional point $\gamma/J = 1$, it is possible to reach the algebraic maximum, i.e., max $K_3 = 3$. We now focus on the initial state and measurement operator dictating the optimization of the temporal correlations leading to this maximization of the LG parameter K_3. For all γ/J, the optimized K_3 values occur when the initial state and the measurement operator are in the $\hat{y} - \hat{z}$ plane, i.e., $\phi = \pi/2 = \phi_m$. This fact implies that all the trajectories followed by the state upon evolution that maximizes K_3 lie on the geodesic in the $\hat{y} - \hat{z}$ plane on the Bloch sphere. Figure 2 shows that the max $K_3 \to 3$ is achieved in narrow slivers of time (deep yellow regions) that bound broad, classical regions with $-3 \leqslant K_3 \leqslant 1$ (deep blue regions). As one approaches the EP, the time at which max K_3 exceeds the traditional quantum bound of $3/2$ also diverges. This divergent time constrains the feasibility of observing these excess correlations in the experiments.

In the $\mathcal{PT}$-symmetric regime, $\gamma/J < 1$, the trajectories on the Bloch sphere are periodic. In this case, we numerically find that the optimal measurement operator $Q = \sigma_y$ is fixed irrespective of non-Hermiticity strength γ/J. Thus, $\theta_m = \pi/2$

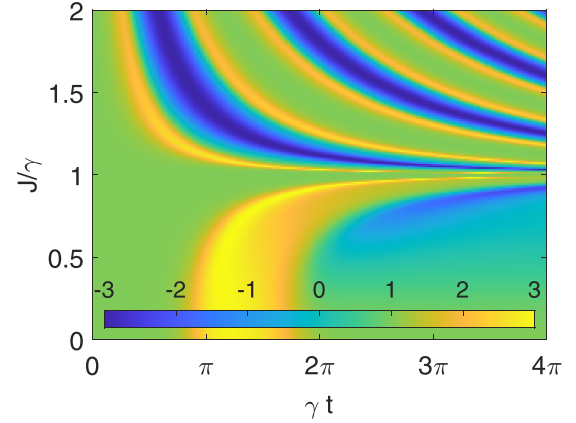FIG. 2. Optimized K_3 for a non-Hermitian qubit as a function of inverse non-Hermiticity J/γ and unitless time γt. We use the gain-loss strength γ as the frequency scale because in the superconducting circuit setup, dynamically tuning it is not easy. In the $\mathcal{PT}$-symmetric region $J/\gamma > 1$, the results are identical to Fig. 1(a), meaning the Lúders bound violation occurs for a fixed dichotomous observable $Q = \sigma_y$ and initial state $|\psi(0)\rangle = |+_y\rangle$. Below the EP at $J = \gamma$, $K_3(t)$ is no longer periodic in time and is maximized when we choose $Q \approx |\epsilon_-\rangle\langle\epsilon_-| - |\epsilon_+\rangle\langle\epsilon_+|$ along the and $|\psi_0\rangle \approx |\epsilon_-\rangle$ in the $\mathcal{PT}$-broken region. Note that the small variance is necessary to perturb $|\psi(0)\rangle$ off the fixed point $|\epsilon_-\rangle$ where $K_3(t) = 1$ is time independent. Larger perturbations lead to max $K_3(t)$ occurring at longer times, albeit with a small decrease in the max K_3 values.

gives the optimal dichotomous observable for all $\gamma/J \leqslant 1$. Fixing the measurement operator establishes a one-to-one correspondence between the choice of the initial state $|\psi\rangle$ dictated by θ and the maximum value of K_3. Moreover, as we approach the EP at $\gamma = J$, the optimal initial state converges to the sole eigenvector of the Hamiltonian $H(\gamma)$ at the EP.

In the $\mathcal{PT}$-broken region, using this choice of the Q and $|\psi\rangle$ gives classical $K_3(t)$ values, as seen in Fig. 1(a). In this region, the two right eigenstates $|\epsilon_\pm\rangle$ of $H(\gamma)$—fixed points of the dynamics—act as the source and the sink, respectively. We find that in this regime it is always possible to access the algebraic maximum of K_3. A remarkable feature of the optimized $K_3(t)$ in the $\mathcal{PT}$-broken region is the broad window of time, near $\gamma t \sim \pi$, where max $K_3(t) > 3/2$ is observed. Traditionally, the $\mathcal{PT}$-symmetry broken region is associated with classical behavior due to the presence of amplifying modes. However, our results in Fig. 2 show that strong temporal quantum correlations exist deep in the $\mathcal{PT}$-broken region where they might be more easily accessible.

In the next section, we present an analytical approach for optimizing K_3 by looking at the Bloch-ball trajectories of quantum states undergoing non-Hermitian dynamics.

III. SPEED OF EVOLUTION ON THE BLOCH SPHERE AND max K_3 DETERMINATION

Note that the two eigenstates of the Hamiltonian $H(\gamma)$, Eq. (1), are fixed points of this dynamics, irrespective of whether the system is in the $\mathcal{PT}$-symmetric phase or $\mathcal{PT}$-broken phase. The nonlinear Bloch equation governing the dynamics of the Bloch vector $\vec{S} = \text{Tr}[\vec{\sigma}\rho(t)]$ corresponding

to Eq. (3) is given by

$$\frac{d\vec{S}(t)}{dt} = \vec{A} \times \vec{S}(t) - \vec{B} + \text{Tr}[\vec{B} \cdot \vec{S}(t)]\vec{S}(t). \tag{11}$$

Here, we have used the generic form of $H(\gamma)$ with arbitrary, real, orthogonal vectors $\vec{A}, \vec{B}$. It represents a TLS with different Rabi drives and dissipation channels. To obtain analytical solutions of Eq. (11), we use the coordinate system defined by the unit vectors $\hat{A}, \hat{B}$ and $\hat{n} = \hat{A} \times \hat{B}$ and obtain

$$\frac{dS_A(t)}{dt} = |B|S_A S_B \tag{12}$$

$$\frac{dS_B(t)}{dt} = -|A|S_n - |B| + |B|S_B^2 \tag{13}$$

$$\frac{dS_n(t)}{dt} = |A|S_B + |B|S_B S_n, \tag{14}$$

where $S_A(t) = \vec{S}(t) \cdot \hat{A}$, $S_B(t) = \vec{S}(t) \cdot \hat{B}$, $S_n(t) = \vec{S}(t) \cdot \hat{n}$. It follows that $S_A = 0$ is constant of motion, and numerical scans shows that max K_3 occurs in the $\hat{B} - \hat{n}$ plane. Therefore, we now work in the $S_A = 0$ subspace. In this subspace, the solutions of Eqs. (13) and (14) are

$$S_B(t) = -\frac{\Omega \sin(\Omega t + C)}{A - B\cos(\Omega t + C)} \tag{15}$$

$$S_n(t) = -\frac{B - A\cos(\Omega t + C)}{A - B\cos(\Omega t + C)}, \tag{16}$$

where $\Omega = \pm\epsilon_\pm = \sqrt{A^2 - B^2}$ is the eigenvalue scale and the constant C is determined by initial conditions $S_B(0)$, $S_n(0)$. We note that when Ω is real ($\mathcal{PT}$-symmetric phase), the dynamics are periodic, whereas when Ω becomes purely imaginary, the periodicity of $S_B(t)$ and $S_n(t)$ is lost and they reach steady-state values at long times.

We can now obtain the SOE of the Bloch vector $\vec{S}$. Using the definition by Anandan and Aharonov [35], we write the change in the state $|\psi(t)\rangle$ in a small time dt as $|\langle\psi(t)|\psi(t + \delta t)\rangle|^2 \equiv 1 - v^2(t)\delta t^2 + O(\delta t^3)$, where $v(t) \equiv \sqrt{v_1^2(t) + v_2^2(t) + v_3^2(t)}$ is the speed of evolution. Note that this speed has units of frequency (or inverse time) because the "distance" it covers on the Bloch sphere is dimensionless. For the non-Hermitian Hamiltonian $H(\gamma)$, Eq. (1), we obtain $v_1^2 = (\Delta\vec{A} \cdot \vec{\sigma})^2$, $v_2^2 = (\Delta\vec{B} \cdot \vec{\sigma})^2$ and $v_3^2 = -i\langle[\vec{A} \cdot \vec{\sigma}, \vec{B} \cdot \vec{\sigma}]\rangle$ [28,31]. We note that although v_1, v_2 are symmetric individual reflections for $\vec{A}$ or $\vec{B}$, v_3 is not. Specializing to our case of a superconducting three-level system, we obtain

$$v_1(t) = \frac{J}{2}\sqrt{1 - S_x^2(t)} \tag{17}$$

$$v_2(t) = \frac{\gamma}{2}\sqrt{1 - S_z^2(t)} \tag{18}$$

$$v_3(t) = \sqrt{\frac{J\gamma}{2}}\sqrt{S_n(t)}, \tag{19}$$

where $\hat{n} = \hat{x} \times \hat{z} = -\hat{y}$. Using Eqs. (17)–(19) above, we obtain the maximum and minimum values for the SOE, namely, $v^{\max} = J + \gamma$ and $v^{\min} = \max(J - \gamma, 0)$. Figure 3 shows the unitless speed of the evolution $v(t)/J$ as a function of the unitless time Jt, with the value of γ/J shown on its corresponding peak, in the $\mathcal{PT}$-broken region. We see that as the system goes deeper into the $\mathcal{PT}$-broken region, the speed increases
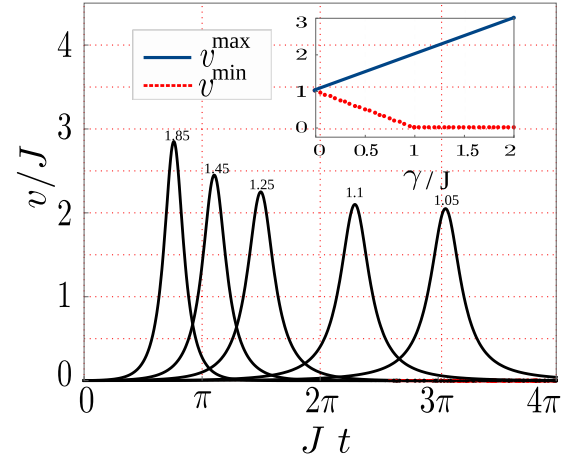

FIG. 3. Speed of evolution $v(t)$ in the $\mathcal{PT}$-broken region shows that its maximum becomes higher and shifts to shorter times as $\gamma/J > 1$ is increased. The value of γ for each curve is shown at its peak. The inset shows $v^{\max}(\gamma) = J + \gamma$ increases linearly with γ, whereas $v^{\min}(\gamma)$ linearly reaches zero at the exceptional point $\gamma = J$.

and its maximum occurs at shorter times. The inset in Fig. 3 shows $v^{\max}(\gamma)$ and $v^{\min}(\gamma)$ are consistent with the analytical results.

To understand the role played by the SOE in maximizing the LG parameter $K_3(t)$, we start with the extreme case, the algebraic bound $K_3 = 3$. Saturating the algebraic bound imposes stringent conditions on the joint probabilities and can only occur when $C_{01} = 1 = C_{12}$ and $C_{02} = -1$. This, in turn, translates to joint probabilities $P_{01}(+1, -1) = 0 = P_{01}(-1, +1)$, $P_{12}(+1, -1) = 0 = P_{12}(-1, +1)$, and $P_{02}(+1, +1) = 0 = P_{02}(-1, -1)$. A typical *gedanken* experiment leading to the LG parameter $K_3 \to 3$ is shown in Fig. 4. Starting from $|+\rangle$, the state $|\psi(t)\rangle$ evolves very little in time t before being projectively measured, leading to $C_{01} \approx 1$. After projective measurement at time t,
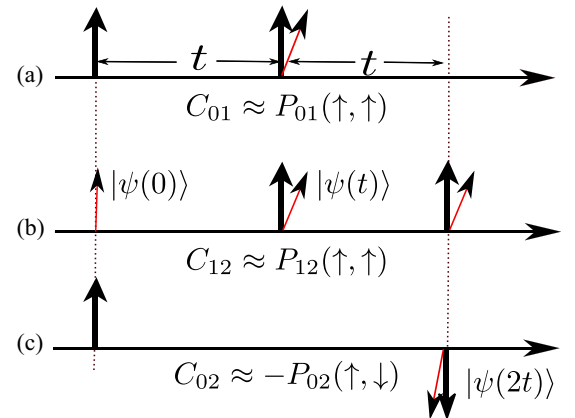

FIG. 4. Schematic of the dynamical process corresponding to the case $K_3 \to 3$. In each correlation C_{01}, C_{12}, or C_{02}, only one of the four joint probabilities survives and the rest are approximated to zero. Black thick arrows represent orthogonal eigenstates of the dichotomous measurement operator Q. In the $\mathcal{PT}$-symmetric phase, $Q = \sigma_y$ is sufficient to maximize K_3 for all γ, whereas in the $\mathcal{PT}$-broken region, the optimal Q is dependent on γ/J.
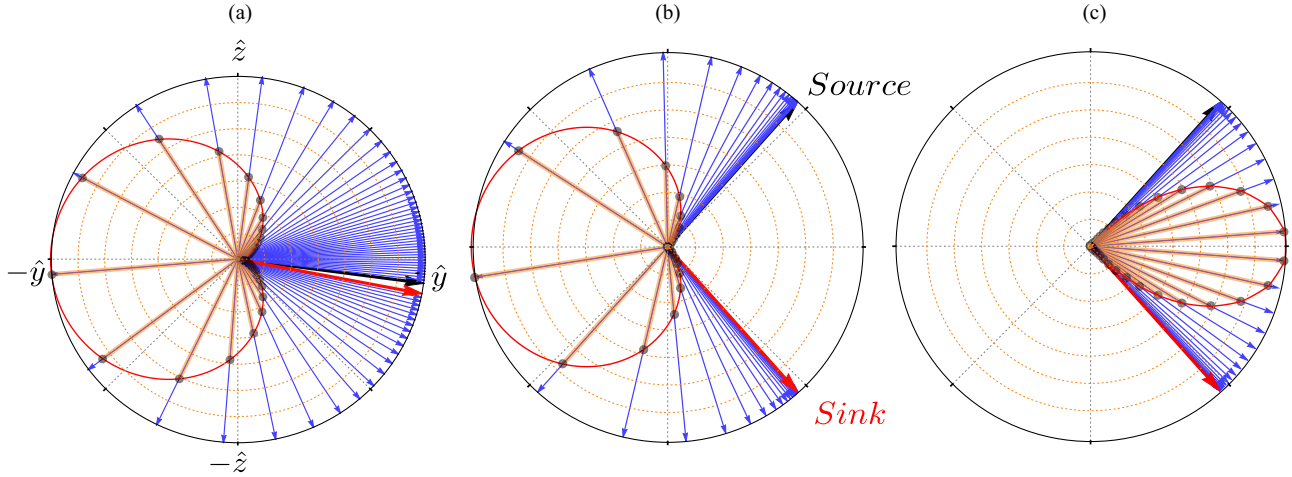
FIG. 5. Time-evolved state $|\psi(t)\rangle$ plotted in the $\hat{y} - \hat{z}$ plane at times $Jt_k = k(Jt)/70$ for a total time interval of $Jt = 10.5$ (blue arrows). Polar plot (orange) shows the corresponding SOE $v(t_k)/v^{\max}$. (a) In the $\mathcal{PT}$-symmetric phase ($\gamma/J = 0.95$), the two fixed points of the dynamics are not along the $\hat{y} - \hat{z}$ great circle. Nonetheless, the speed of evolution is maximum when $|\psi(t)\rangle = |-_y\rangle$. (b and c) In the $\mathcal{PT}$-broken region, $\gamma/J = 3$, the fixed points of the dynamics in the $\hat{y} - \hat{z}$ plane are shown by "source" ($|\epsilon_-\rangle$) and "sink" ($|\epsilon_+\rangle$). The initial state is on the longer arc joining them ($\theta = 0.728$ and $\phi = 3\pi/2$) in (b) and it is along the shorter arc ($\theta = 0.732$ and $\phi = 3\pi/2$) in (c). Polar plots: Also plotted are the respective SOEs $v(t)/v^{\max}$.

it evolves further to time $2t$, where another projective measurement leads to $C_{12} \approx 1$. On the other hand, when the initial state is allowed to evolve uninterrupted to time $2t$, anticorrelated dynamics are observed when projectively measured at time $2t$, i.e., $C_{02} \approx -1$. This sort of nonuniform in time dynamics, made possible by rapidly varying SOE, underpins the extreme temporal correlations in the $\mathcal{PT}$-symmetric region, shown in Fig. 1(a) [28].

The more-than-Lüder correlations in the $\mathcal{PT}$-symmetry broken regions arise as follows. The $|\epsilon_+\rangle$ eigenstate in the $\mathcal{PT}$-broken region denotes an "amplifying mode," and therefore a stable fixed point (sink) towards which all states on the Bloch sphere flow to. In contrast, the $|\epsilon_-\rangle$ state, denoting the "decaying mode," represents an unstable fixed point (source). Starting with $|\psi(0)\rangle \approx |\epsilon_-\rangle$, the system slowly departs the neighborhood of the source and its speed on the Bloch sphere increases as the system gets farther away from the source fixed point to the sink fixed point.

In order to illustrate the above points we consider explicit examples where $K_3 \to 3$ in the PT-symmetric regime and $\mathcal{PT}$ broken regime. As mentioned earlie,r the trajectories followed by the initial state lie on the $\hat{y} - \hat{z}$ plane geodesic of the Bloch sphere. In Fig. 5, we show the time-evolved state $|\psi(t)\rangle$ (blue arrows) at times $Jt_k = k(10.5/70)$ for $k = 0, \ldots, 70$, with initial state ($k = 0$) in black and final state ($k = 70$) in red. Overlaid on it is the polar plot of the corresponding SOE $v(t)$ normalized to its maximum value $v^{\max}(\gamma)$. Figure 5(a) shows representative results in the $\mathcal{PT}$-symmetric phase ($\gamma/J = 0.95$). In the $\mathcal{PT}$-broken region, there are two unequal arcs that connect the source ("lossy") state $|\epsilon_-\rangle$ to the sink ("gain") state $|\epsilon_+\rangle$. Figure 5(b) shows representative results when the initial state is along the longer arc, whereas results for an initial state along the shorter arc are in Fig. 5(c). These results are for $\gamma/J = 3$, i.e., deep in the $\mathcal{PT}$-broken region. It is important to note that the LG parameter K_3 is very sensitive to location of the initial state $|\psi\rangle \approx |\epsilon_+\rangle$; in

particular, choosing any initial state on the shorter arc cannot lead to max $K_3 \to 3$.

IV. EFFECTS OF OTHER LINDBLAD DISSIPATORS

Until now, we have focused on the coherent dynamics of an effective two-level system that arises from a non-Hermitian Hamiltonian and a norm-preserving nonlinearity, Eq. (3). In reality, however, a dispersively coupled superconducting circuit with three levels, postselected to the top two levels $\{|f\rangle, |e\rangle\}$, is affected by spontaneous emission decay from $|f\rangle$ to $|e\rangle$, as well as phase noise affecting the two levels. In the Lindblad formalism, these correspond to dissipators

$$L_{ef} = |e\rangle \langle f| = \begin{pmatrix} 0 & 0 & 0 \\ 1 & 0 & 0 \\ 0 & 0 & 0 \end{pmatrix}, \quad (20)$$

$$L_\phi = |f\rangle \langle f| - |e\rangle \langle e| = \begin{pmatrix} 1 & 0 & 0 \\ 0 & -1 & 0 \\ 0 & 0 & 0 \end{pmatrix}, \quad (21)$$

with strengths γ_{ef} and γ_ϕ, respectively. We obtain the 2×2 density matrix $\rho(t)$ by solving for the full 3×3 density matrix $\rho_3(t)$ and postselecting on trajectories with no quantum jumps from $|e\rangle$ to the ground state $|g\rangle$.

Figure 6(a) reproduces the optimized max $K_3(J/\gamma, \gamma t)$ in Fig. 2 when $\gamma_{ef} = 0 = \gamma_\phi$. When $\gamma_{ef}/\gamma = 10^{-2}$ is nonzero, the EP at $\gamma = J$ is washed out [27], and correspondingly the max K_3 that occurs along that line is suppressed from its algebraic maximum [Fig. 6(b)]. It is remarkable, however, that the K_3 excess deep in the $\mathcal{PT}$-broken region remains robust. Qualitatively similar behavior is observed in the presence of phase noise with $\gamma_\phi/\gamma = 10^{-2}$ [Fig. 6(c)]. These results suggest that the best chance of observing beyond-Lüder temporal correlations, quantified by $K_3 > 3/2$, is not in the $\mathcal{PT}$-symmetric region or at the EP, but instead in the $\mathcal{PT}$-broken region.
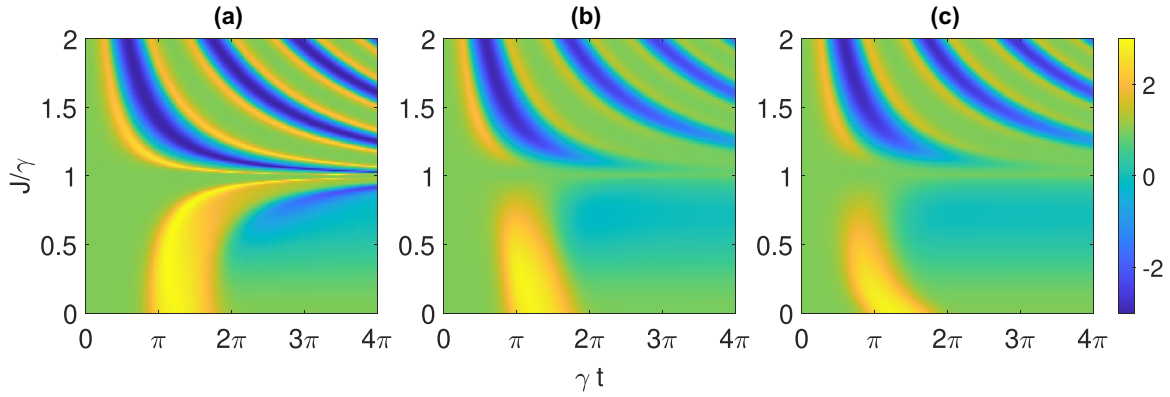
FIG. 6. Effects of spontaneous emission dissipator L_{ef} and the phase noise dissipator L_ϕ within the $\{|e\rangle - |f\rangle\}$ submanifold on the optimized LG parameter $K_3(J/\gamma, \gamma t)$. (a) Optimized max K_3 from Fig. 2 in the "clean limit." (b) When $\gamma_{ef}/\gamma = 10^{-2}$, the temporal correlations near the EP $\gamma = J$ are suppressed while those in the deep $\mathcal{PT}$-broken region survive. (c) When $\gamma_\phi/\gamma = 10^{-2}$, again, the temporal correlations near the EP are suppressed. In both cases, the larger-than-Lüder K_3 values remain robust deep in the $\mathcal{PT}$-broken region with $J/\gamma \sim 0.4$ and $\gamma t \sim \pi$, thereby supporting the feasibility of observing them in experiments.

V. DISCUSSION AND CONCLUSION

In this paper, we have investigated the temporal correlations quantified in terms of LG parameter K_3 for a single two-level system governed by a non-Hermitian, $\mathcal{PT}$-symmetric Hamiltonian across its exceptional point. We found that max $K_3(J/\gamma, \gamma t)$ exceeds the Lüder bound of $3/2$ and approaches its algebraic bound of 3 over wide domain in the $\mathcal{PT}$-broken region given by $J/\gamma < 1$. In contrast, earlier studies have predicted beyond-Lüder max K_3 only in the $\mathcal{PT}$-symmetric region, approaching the algebraic limit at divergent times $\gamma t \gg 1$ at the EP $J = \gamma$.

We have shown that the extreme violation of LGI is caused by a nonuniform speed of evolution SOE that results from the nonlinear equation of motion, Eq. (2). More precisely, a dynamics where a state evolves with minimum SOE during the initial time t and then maximum SOE during time between t and $2t$ gives rise to extreme temporal correlations. Our findings thus also imply that $v^{\min} = \max(0, J - \gamma)$ can act as an "order parameter" that indicates $\mathcal{PT}$-symmetric phase.

We note that our key result—LG parameter K_3 exceeding the Lüder bound of $3/2$ due to the nonuniform SOE on the Bloch sphere—is independent of whether violation of LGI, defined by $K_3 > 1$, is a signature of quantum behavior. For completeness, we recall the loopholes accompanying the interpretation $K_3 > 1$ as a marker of quantum dynamics. Recently, alternative approaches have been proposed to deal with the noninvasive measurability loophole [36,37] and the clumsiness loophole [38]. Our discussion here is restricted to only the *statistical version* of noninvasive measurability (NSIT) and arrow of time (AoT) conditions.

Recall that simultaneous nonviolation of NSIT and AoT conditions guarantees the existence of a global probability distribution [11] that implies macroscopic realism. In unitary dynamics, (one or more of) NSIT conditions are violated, while all the AoT conditions are satisfied. Consider the dynamical process, governed by the coherent, non-Hermitian evolution, in Fig. 4. In this case, through explicit calculations we find that (a) all two-time AoT conditions are satisfied, (b) three-time AoT conditions of types $\text{AoT}_{01(2)}$: $P_{01}(a, b) = \sum_{c=\pm 1} P_{012}(a, b, c)$ and $\text{AoT}_{0(12)}$: $P_0(a) = \sum_{b,c=\pm 1} P_{012}(a, b, c)$ are also satisfied, and (c) all the NSIT conditions of type $\text{NSIT}_{(0)12}$: $P_{12}(b, c) = \sum_{a=\pm 1} P_{012}(a, b, c)$ are also satisfied owing to the preparation of the initial state as an eigenstate of the measurement operator. However, the NSIT conditions of type

$$\text{NSIT}_{0(1)2} : P_{02}(a, c) = \sum_{b=\pm 1} P_{012}(a, b, c) \qquad (22)$$

are not satisfied in general. Following the necessary and sufficient conditions for macroscopic realism (MR) [11],

$$\text{MR} \Leftrightarrow \text{NSIT}_{(0)1} \wedge \text{NSIT}_{0(1)2} \wedge \text{NSIT}_{(0)12} \wedge \text{AoT}_{01(2)}, \quad (23)$$

we find that postselected non-Hermitian dynamics presented here is inconsistent with MR, just as unitary quantum dynamics is inconsistent with MR.

[1] C. Emary, N. Lambert, and F. Nori, Rep. Prog. Phys. **77**, 016001 (2014).

[2] J. S. Bell, *Speakable and Unspeakable in Quantum Mechanics: Collected Papers on Quantum Philosophy* (Cambridge University Press, Cambridge, 2004).

[3] A. Peres, Found. Phys. **29**, 589 (1999).

[4] A. J. Leggett and A. Garg, Phys. Rev. Lett. **54**, 857 (1985).

[5] A. J. Leggett, J. Phys.: Condens. Matter **14**, R415 (2002).

[6] A. J. Leggett, Rep. Prog. Phys. **71**, 022001 (2008).

[7] J. P. Paz and G. Mahler, Phys. Rev. Lett. **71**, 3235 (1993).

[8] W. Son, J. Lee, and M. S. Kim, Phys. Rev. Lett. **96**, 060406 (2006).

[9] C. Budroni, T. Moroder, M. Kleinmann, and O. Gühne, Phys. Rev. Lett. **111**, 020403 (2013).

[10] J. Kofler and C. Brukner, Phys. Rev. A **87**, 052115 (2013).

[11] L. Clemente and J. Kofler, Phys. Rev. A **91**, 062103 (2015).

[12] A. Palacios-Laloy, F. Mallet, F. Nguyen, P. Bertet, D. Vion, D. Esteve, and A. N. Korotkov, Nat. Phys. **6**, 442 (2010).

[13] G. C. Knee, K. Kakuyanagi, M.-C. Yeh, Y. Matsuzaki, H. Toida, H. Yamaguchi, S. Saito, A. J. Leggett, and W. J. Munro, Nat. Commun. **7**, 13253 (2016).

[14] X. Liu, Z.-Q. Zhou, Y.-J. Han, Z.-F. Li, J. Hu, T.-S. Yang, P.-Y. Li, C. Liu, X. Li, Y. Ma, P.-J. Liang, C.-F. Li, and G.-C. Guo, Phys. Rev. A **100**, 032106 (2019).

[15] K. Joarder, D. Saha, D. Home, and U. Sinha, PRX Quantum **3**, 010307 (2022).

[16] T. Fritz, New J. Phys. **12**, 083055 (2010).

[17] C. Budroni and C. Emary, Phys. Rev. Lett. **113**, 050401 (2014).

[18] V. Gorini, A. Kossakowski, and E. C. G. Sudarshan, J. Math. Phys. **17**, 821 (1976).

[19] G. Lindblad, Commun. Math. Phys. **48**, 119 (1976).

[20] T. Baumgratz, M. Cramer, and M. B. Plenio, Phys. Rev. Lett. **113**, 140401 (2014).

[21] S. L. Braunstein and P. van Loock, Rev. Mod. Phys. **77**, 513 (2005).

[22] K. Modi, A. Brodutch, H. Cable, T. Paterek, and V. Vedral, Rev. Mod. Phys. **84**, 1655 (2012).

[23] F. Caruso, V. Giovannetti, C. Lupo, and S. Mancini, Rev. Mod. Phys. **86**, 1203 (2014).

[24] L.-H. Shao, Z. Xi, H. Fan, and Y. Li, Phys. Rev. A **91**, 042120 (2015).

[25] D. Manzano, AIP Adv. **10**, 025106 (2020).

[26] S. Ghosh, A. V. Varma, and S. Das, J. Phys. A: Math. Theor. **56**, 205302 (2023).

[27] M. Naghiloo, M. Abbasi, Y. N. Joglekar, and K. W. Murch, Nat. Phys. **15**, 1232 (2019).

[28] A. V. Varma, I. Mohanty, and S. Das, J. Phys. A: Math. Theor. **54**, 115301 (2021).

[29] H. S. Karthik, H. A. Shenoy, and A. R. U. Devi, Phys. Rev. A **103**, 032420 (2021).

[30] J. Naikoo, S. Kumari, S. Banerjee, and A. K. Pan, J. Phys. A: Math. Theor. **54**, 275303 (2021).

[31] D. C. Brody and E.-M. Graefe, Phys. Rev. Lett. **109**, 230405 (2012).

[32] J. Gunderson, J. Muldoon, K. W. Murch, and Y. N. Joglekar, Phys. Rev. A **103**, 023718 (2021).

[33] S. Rotter, Nat. Phys. **15**, 1214 (2019).

[34] M. A. Quiroz-Juárez, A. Perez-Leija, K. Tschernig, B. M. Rodríguez-Lara, O. S. M. na Loaiza, K. Busch, Y. N. Joglekar, and R. de J. León-Montiel, Photon. Res. **7**, 862 (2019).

[35] J. Anandan and Y. Aharonov, Phys. Rev. Lett. **65**, 1697 (1990).

[36] S.-S. Majidy, H. Katiyar, G. Anikeeva, J. Halliwell, and R. Laflamme, Phys. Rev. A **100**, 042325 (2019).

[37] A. K. Pan, Phys. Rev. A **102**, 032206 (2020).

[38] E. Huffman and A. Mizel, Phys. Rev. A **95**, 032131 (2017).